ELSEVIER

Journal of Fluids and Structures 19 (2004) 815–833

JOURNAL OF FLUIDS AND STRUCTURES

www.elsevier.nl/locate/jnlabr/yjfls

Three-dimensional nature of vortices in the near wake of a wavy cylinder

K. Lam[a,*], F.H. Wang[b], R.M.C. So[a]

[a] *Department of Mechanical Engineering, The Hong Kong Polytechnic University, Hung Hom, Kowloon, Hong Kong*
[b] *School of Energy and Power Engineering, Xi'an Jiaotong University, Xi'an, PR China*

Received 8 January 2003; accepted 6 April 2004

Abstract

The near wake of a wavy cylinder has been experimentally investigated using various techniques, including Laser Doppler Anemometer, Laser-Induced Fluorescence Visualization and Digital Particle Image Velocimetry. The work aims to provide understanding to the mechanism of the cross-flow around a wavy cylinder as well as to comprehend why the introduction of relatively small degrees of spanwise waviness could have a significant effect on drag reduction and a corresponding suppression of cylinder vibration. Distributions of the mean and fluctuating velocity components along the streamwise, spanwise and transverse direction are presented. The development of the flow patterns and the corresponding vortex interactions are obtained by flow visualization. The experimental results indicated that the average vortex formation length behind the wavy cylinder is longer than that behind the circular cylinder. It appears that there is a direct link between the long formation length and drag reduction and vibration suppression. For the wavy cylinder, the wake on the saddle plane has a longer vortex formation region and a more rapid reverse flow, as well as being wider than that on the nodal plane. Furthermore, the spanwise flow is from the saddle plane towards the nodal plane on both sides of the wavy cylinder. It was deduced that the free shear layers shed from the points near the saddles extend along the spanwise direction, while the shear layers near the nodes contract. The turbulence correlations show that the vortex streets in the circular cylinder wake are more regular, while the wavy cylinder wake shows more incoherent turbulence due to enhanced turbulent mixing; a consequence of three-dimensional (3-D) effects. The mean velocity and turbulence data also provide an important database for the validation of turbulence modelling and 3-D numerical simulations.

1. Introduction

Vortex shedding is an important feature of bluff body aerodynamics. The shedding of vortices and their dynamics are believed to play a governing role in many features of the flow, such as fluid mixing, heat transfer, and noise generation. The wake vortices can generate large unsteady forces, which have the potential to damage the structural integrity of bluff bodies. For this reason, many methods have been proposed in recent years to control the dynamics of the wake vortex with the aim to suppress vortex shedding and to reduce the magnitude of the fluctuating lift force as well as that of the mean drag.

One approach in these studies is to introduce some forms of three-dimensional (3-D) geometric disturbance to the base form of a nominally two-dimensional (2-D) bluff body. For example, Naumann et al. (1966) varied the separation

*Corresponding author. Tel.: +852-27666649; fax: +852-2365470.
E-mail address: mmklam@polyu.edu.hk (K. Lam).

0889-9746/$ - see front matter © 2004 Elsevier Ltd. All rights reserved.
doi:10.1016/j.jfluidstructs.2004.04.004

position along a circular cylinder by attaching short lengths of wire fixed alternately at two angular positions across the span. It was reported that this suppressed vortex shedding. Following this idea of breaking the separation line, a number of researchers, including Tanner (1972), Rodriguez (1991) and Petrusma and Gai (1994), have studied the reduction of the drag of blunt-trailing-edge wings by introducing a segmented trailing edge. The maximum drag reduction obtained using this method was 64%. However, no explanation of the aerodynamic mechanisms, which are responsible for the drag reduction, was given. The experiments of Tombazis and Bearman (1997), and Bearman and Owen (1998) were carried out to study the 3-D features found in the wakes of nominally 2-D bluff bodies known as vortex dislocations. These are associated with spanwise changes in vortex shedding frequency and they provide a means by which vortices from adjacent cells, shedding at different frequencies, can join together. They also found that for a 2-D body, dislocations appear apparently randomly in time and in spanwise position. In order to fix the dislocation positions, a spanwise wavy trailing edge was introduced. It was also observed in their experiments that, due to the influence of this wavy edge, the base pressure increased. Generally, an increase in base pressure leads to a decrease in the mean drag. As pointed out by Owen and Bearman (2001), vortex shedding from bluff bodies can be weakened and in some cases suppressed when the flow separation lines are forced to be sinuous.

Based on the ideas discussed above, a circular cylinder with varying cross-section along the spanwise direction is introduced. This cylinder is termed a "wavy cylinder" and could be used to reduce drag and to weaken or suppress vortex shedding. The geometry of this cylinder is shown in Fig. 1. In a previous experimental investigation (Lam et al., 2004), it was found that, comparing with a uniform circular cylinder, a drag reduction up to 20% was obtained in a Reynolds number (Re) range of 10 000 to 60 000. The flow-induced vibration (FIV) was also reduced significantly (a reduction of r.m.s. lift force coefficient from 0.87 to 0.10 at resonance was measured). Despite the fact that some salient features of the induced forces were obtained, an understanding of the wake flow behind the wavy cylinder has not been achieved.

Another motivation for the present study is the lack of detailed experimental measurements of the velocity field and turbulence intensities in the near wake of a cylinder. An accurate and reliable data set could serve as a benchmark for turbulence modelling validation. In the last decade, there is a surge of studies on the 3-D instability behind a cylinder using numerical simulation (Braza et al. 2001; Zhang and Dalton 1998). However, as mentioned by Yang and Zebib (1989), some 3-D numerical simulation results were only validated against sparsely measured velocity profiles in the near wake. Consequently, these studies could not be used to extract a deep understanding of the fundamental nature of unsteady separated flows, particularly those containing several multiple instabilities. The wavy cylinder is a natural 3-D extension of the well-documented circular cylinder and is a good benchmark for the validation of numerical simulations. Furthermore, the flow field behind a wavy cylinder has some interesting 3-D characteristics; therefore, the flow around a wavy cylinder offers a unique unsteady, large-scale, 3-D wake for detailed investigation.

In the literature, few studies have been presented on flow around wavy cylinders. Howarth (1951) derived the boundary layer equations in general surface-fitted coordinates. Davey (1961) studied the flow of a viscous incompressible fluid in the immediate neighborhood of a saddle point of attachment. Cooke and Robins (1970)

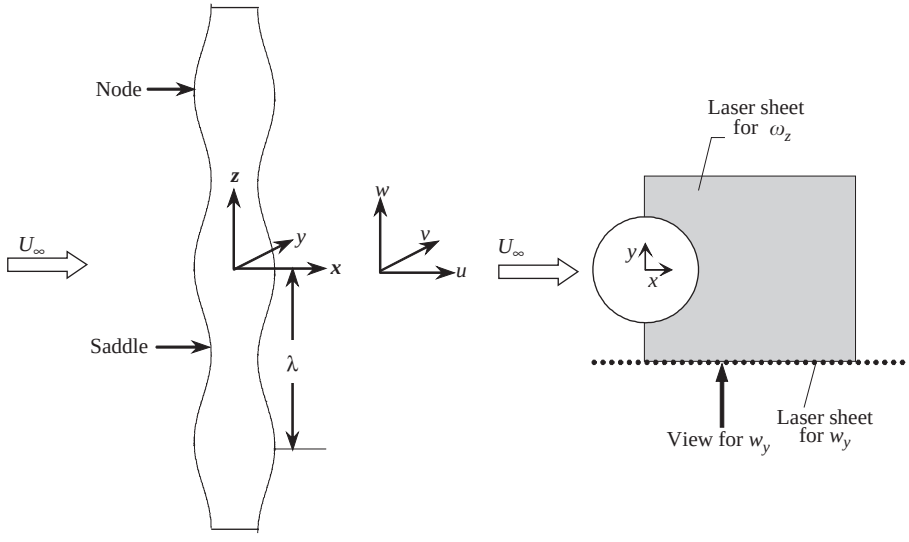

Fig. 1. The geometry of the wavy cylinder and orientations of the laser sheets.

solved the boundary layer flow between nodal and saddle points of attachment using a finite difference method. Duck (1979) investigated the flow induced by a torsionally oscillating wavy cylinder at a Taylor number close to its critical value, and the interaction between the forced and natural solutions. The results of the above investigations show that, for sufficiently small waviness, the entire boundary layer flows from the geometric nodal point to the geometric saddle point without separation. Kerczek (1988) predicted that a reversed flow would occur (directed away from the saddle and towards the nodal point), but that it would be limited to the bottom of the boundary layer, hence would not disrupt the outer flow. Keser et al. (2001) used a 3-D discrete vortex method to simulate the separated flow around a circular cylinder with sinusoidal waviness along its span. However, all the above studies were based on various assumed forms for the flow field from the nodal to the saddle point of attachment.

In the experimental area, Ahmed and Bays-Muchmore (1992) measured the surface-pressure distributions of a set of wavy cylinders with different axial wavelengths based on the mean cylinder diameter, d. The Re in their experiment was 20 000 and the mean static pressure data was determined using linear interpolation. Their results showed that the separated flow structures near the geometric nodes were distinctly asymmetric for a large fraction of time, and the sectional drag coefficients at the geometric nodes are greater than at the geometric saddle. In another study, Ahmed et al. (1993) explored the effects of 3-D separation line topology on the development of the wavy turbulent wake. As a result, they found that the formation of trailing streamwise vortices behind nodal points of separation gave rise to a locally narrower wake, a rapid wake velocity recovery and a suppression of the turbulence development within the separated boundary layer.

In this investigation, the streamwise, transverse and spanwise velocity components in the near wake of a wavy cylinder were measured using the laser doppler velocimetry (LDV) technique. This technique can provide accurate and reliable data compared to those obtained using a conventional hot-wire technique, especially inside the highly turbulent and recirculating region (Crickmore et al. 1999). As a baseline for comparison, a stationary circular cylinder at approximately the same Re was also studied. Furthermore, a detailed flow visualization study carried out with the aid of laser-induced fluorescence (LIF) and particle image velocimetry (PIV) on flow patterns in the near wake was also conducted. Just as pointed out by Sumner et al. (2000), determining the fluid behavior from measured quantities is prone to misinterpretation, particularly when it was carried out without the benefit of flow visualization. It is hoped that the present experiments could lead to an understanding of the mechanism of the cross-flow around a wavy cylinder while, at the same time, provide a database for the validation of computational fluid dynamics (CFD) software. The data could also be used to extract information on why a relatively small degree of spanwise waviness could give rise to a relatively large drag reduction and a corresponding suppression of cylinder vibration.

2. Experimental details

The geometry of the wavy cylinder is described by the equation, $d_z = d + 2a\cos(2\pi z/\lambda)$. Here, d_z is the local diameter, d is the mean diameter, a is the amplitude of the surface curve, λ is the wavelength, and z is the spanwise location. The terminology used to describe the wavy cylinder is defined in Fig. 1. The axial locations of the maximum diameter are hereafter termed "nodes", while the axial locations of the minimum diameter are denoted as "saddles". The origin of the coordinate is located at the center of a nodal cross-section. The dimensionless parameters of the wavy cylinder were chosen as $a/d = 0.091$ and $\lambda/d = 2.273$, because they were found to be more effective in producing the measurable drag reduction and vibration suppression [Lam et al. (2004)]. For comparison, a circular cylinder with $d = 12.7$ mm was also used in the LDA measurements.

2.1. LDA measurements in the wind tunnel

The LDA measurements were carried out in a closed-circuit wind tunnel with a working square cross-section (0.6 m × 0.6 m) and a length of 2.0 m, including the x (streamwise), y (transverse) and z (spanwise) velocity measurements. The test-section is made of Perspex. The velocity in the test-section could be continuously varied from 0 to 50 m/s by an inverter, which controls the rotation speed of the wind tunnel fan. The boundary layer on the wall at the location where the cylinder was introduced was measured to be about 20 mm thick, while the free-stream turbulent intensity was measured to be less than 0.2%. The cylinder spanned the full width of the working section with a maximum blockage of about 5.5% and an aspect ratio of 18.2.

In order to obtain the mean and fluctuating velocity information, a two-color fiber-optic LDA with a focal length of 310 mm was employed. The green (wavelength = 514.5 nm) and the blue (wavelength = 488 nm) coherent light of an Argon-ion laser were used. The LDA was operated in the backscatter mode and with a frequency shift. The probe with a beam expander having a factor of 1.94 contained both transmitting and receiving optics. The signals from the

photomultipliers were analyzed using a correlation-technique LDA signal processor (DANTEC model 58N40 two-component LDA with enhanced FVA signal processor). The LDA system comes with the software for data processing and analysis. The measuring volume has a minor axis of 1.18 mm and a major axis of 2.48 mm. Thus, the measured mean velocity was estimated to have an error $<3\%$ and the corresponding error for the measured root mean square (r.m.s.) value was less than 10%. The seeding droplets (Invent Safex-Inside-Nebelfluid SUPER) were generated using a Dantec SAFEX 2010 fog generator, which was located downstream of the cylinder. It is worth pointing out that a three-component lightweight traverse equipped with the necessary hardware and software forms a part of the main system, where the optical head of the LDA is fixed. The traverse has a positioning accuracy of about 35 μm with a resolution of about 2 μm. Therefore, the profiles of the mean velocity, and the normal and shear stresses along the x, y and z direction could be achieved simultaneously and automatically by sampling the data following the x, y and z coordinate sequence.

2.2. Flow visualization in the water tunnel

The flow visualization experiments were carried out in a low speed closed-loop water tunnel with a working section of 150 mm × 150 mm cross-section and 500 mm in length. The walls of the test-section were made of acrylic and glass plates so that they were transparent for laser diagnostics and visualization techniques. The velocity in the working section could be continuously varied from 0 to 0.35 m/s by an inverter. The cylinder model was made of acrylic and positioned in the middle of the working section to minimize near-wall effects. The wavy cylinder model with a blockage of 11.7% was installed on a turntable circular plate in a cantilevered manner and the clearance between the ends of the cylinders and the sidewalls of the test-section was about 1 mm. To estimate the effects of blockage and clearance on the visualization results, a series of experiments was carried out using a set of circular cylinders with different blockages and clearances. It was found that similar results could be obtained when the blockage was less than about 15% and the clearance was less than about 5 mm. Hence, the effects of blockage and clearance on the visualization results could be neglected when the blockage is 11.7% and the clearance is 1 mm. Mounting facilities were provided in one of the vertical walls at the measuring station, so that the plate could be flush mounted with the surface of the wall. The Re was based on d and the free-stream velocity, U_∞.

In order to measure the instantaneous velocity field and to calculate the vorticity field, a digital PIV method was employed. The water flow was seeded with particles made of polyamide. These particles are white PSP "hollow" microspheres with a mean diameter <50 μm. A 4W Spectra-Physics Stabilite 2017 Argon-Ion laser was used to illuminate the near wake region behind the cylinder. The laser beam was pulsed using a scanning beam box, including a circular mirror, a rotating polygon mirror and a parabolic reflecting mirror. The scanning frequency of the laser sheet is continuously varied in the range of 1.0–12.7 ms. The digital images were recorded using an Adimec MX12P CCD camera with 1024 × 1024 pixels resolution and a Matrox Pulsar frame grabber. The maximum frame rate is 25 images per second. The cross-correlation technique of the multi-frame single exposure method was adopted. The velocity field was extracted from the particle image using an VIDPIV software based on the Young's fringe method.

Laser-induced fluorescence (LIF) was also used in the experiments to examine the development of the flow patterns and the corresponding vortex interactions. The florescent dye used is Rhodamine 6G (99%) with a maximum absorption wavelength of 530 nm and a maximum emission wavelength of 560 nm. The dye ejected from the holes on the cylinder was illuminated using the same laser sheet and recorded with a JVC CCD video camera. The frame rate of this video camera is 25 f/s.

3. Results and discussion

3.1. Wake centerline velocity and vortex formation length

Longitudinal evolution of the normalized mean velocity (U/U_∞) and normalized r.m.s. values of the fluctuating streamwise velocity ($u_{\mathrm{RMS}}/U_\infty$) along the wake centerline ($y=0$ plane) of the wavy cylinder and a circular cylinder at Re = 3000, 6000 and 9000 are shown in Fig. 2. The typical curve for a circular cylinder at Re = 3000, 5000, and 8000 obtained by Norberg (1998) is also plotted in the figure for comparison with the present measurements. The flow direction is from left to right. In the present study, all lengths are normalized by d or by the wavelength, λ. From Fig. 2, it can be seen that there is a small disparity between the present results and those of Norberg (1998), which may be due to a combination of effects related to Re, notable differences in aspect ratio, free-stream conditions, blockage ratio, etc. From the results, it can be observed that, starting from the base of the cylinder at $x/d=0.5$, the near wake flow field changed from forward flowing into a reverse flow region. With a different recovery rate, the streamwise velocity component gradually increased to about 0.8 at $x/d=10$ from a minimum as low as -0.5. The velocity recovery speed is

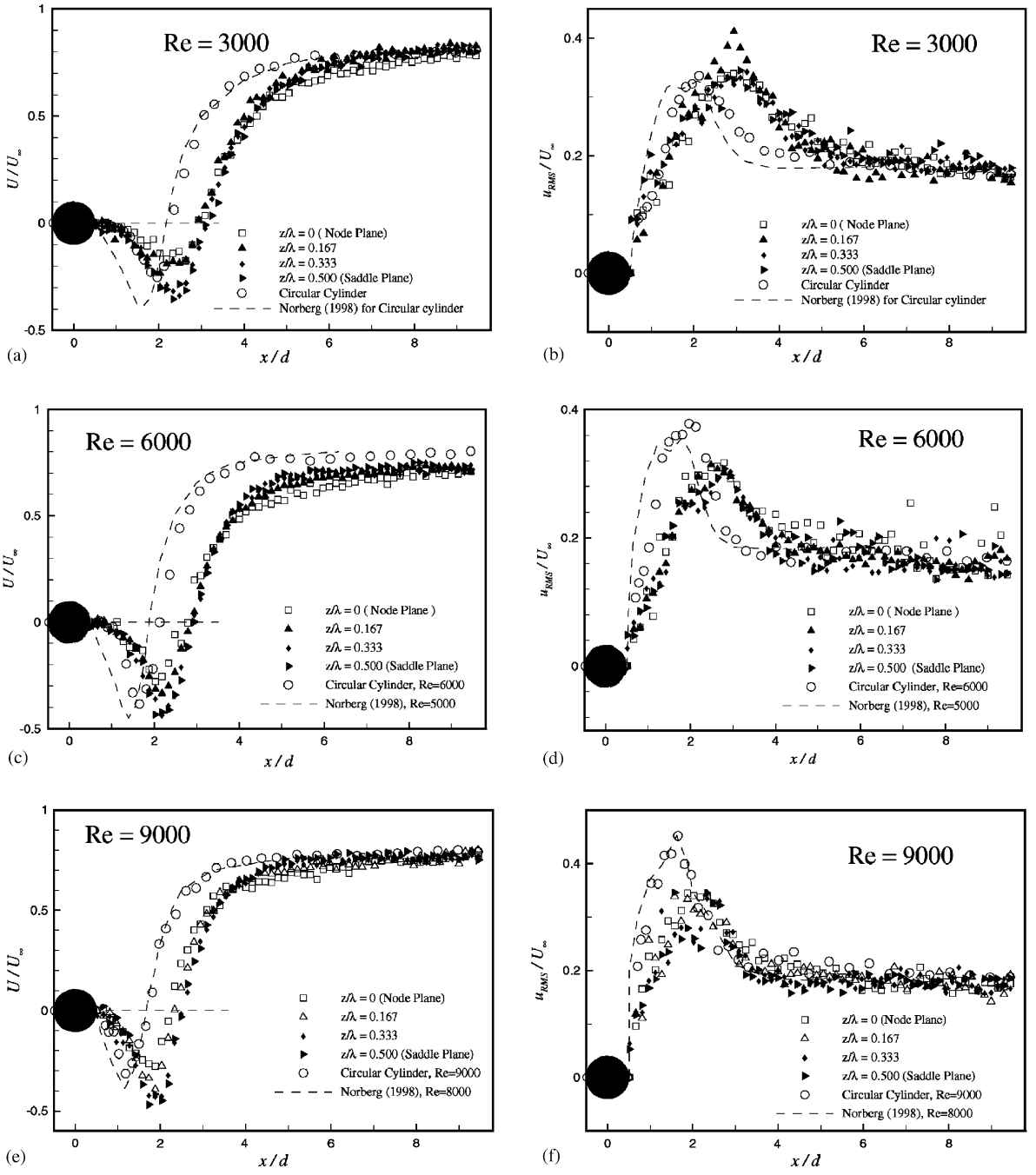

Fig. 2. LDA results from measurements along the wake centerline. (a) Mean streamwise velocity, Re = 3000, (b) r.m.s. streamwise velocity, Re = 3000, (c) mean streamwise velocity, Re = 6000, (d) r.m.s. streamwise velocity, Re = 6000, (e) mean streamwise velocity, Re = 9000, (f) r.m.s. streamwise velocity, Re = 9000.

related to the von Karman vortex formation region. Therefore, it is necessary to deduce the vortex formation length from these measurements. It may not be possible to deduce an empirical expression for the vortex formation length because definitions for the length varied among author. For instance, Bloor (1966) defined the formation length as the point where low frequency irregularities suddenly decreased in intensity; Gerrard (1978) used dye to trace the point where irrotational flow crossed the wake centerline; Woo et al. (1983) and Norberg (1986) used a hot-wire to locate the

r.m.s. maximum of the second harmonic of the fluctuating velocity on the axis of the wake. The formation length has also been associated with the point on the wake centerline where the streamwise Reynolds normal stress reaches a maximum [Norberg (1998); Govardhan (2001)]. Furthermore, the location of the time-averaged closure point (point of zero U/U_∞ on the wake centerline) has been used to measure the formation length. In the present study, both the wake closure length (L_{fc}) and the location along the wake centerline where $u_{\mathrm{RMS}}/U_\infty$ reaches a maximum (L_{fu}) are used to estimate the vortex formation length. The values thus determined for the circular and wavy cylinder are listed in Table 1 for comparison.

There is a decrease of about 24% in L_{fc} for the circular cylinder as Re increases from 3000 to 9000; L_{fu} followed the same pattern as L_{fc} although its magnitude of decrease is different. A similar behavior is also observed for the wavy cylinder. Even though the reverse flow region behind the wavy cylinder is longer than that of the circular cylinder, the results in Table 1 seem to show that the rate of decrease with Re is about the same for the same Re range. The highest $u_{\mathrm{RMS}}/U_\infty$ always occurs slightly upstream of the mean wake closure point [Norberg (1998)], where the mean separating streamline meets the wake centerline and the vortices are closest to the wake centerline. Therefore, L_{fu} is always less than L_{fc}. Noca (1998) classified the closure point region as Region 2, believing that the location of the maximum $u_{\mathrm{RMS}}/U_\infty$ along the wake centerline lies somewhere between Region 1 and Region 2. In comparison with the circular cylinder, the formation region of the wavy cylinder is much longer; for example, there is an increase of about 31.6% at the nodal plane and an increase of 38.7% at the saddle plane in L_{fc} at $\mathrm{Re}=3000$. As pointed out by Bearman (1965), the formation length is approximately inversely proportional to the base suction coefficient for a circular cylinder, i.e. $L_f = C/(-C_{pb})$. The C value is in the range of 1.6–1.8 in the Re range from 1000 to 9000. This implies that L_f is sensitive to important parameters defining the problem, and so analogously should C_{pb}. The same conclusion can be drawn for the case of a wavy cylinder as illustrated by the previous measurements of Lam et al. (2004) and the present results. For example, at $\mathrm{Re}=36\,000$, $C_{pb}=-1.28$ for a circular cylinder; this changes to $C_{pb}=-0.98$ in a nodal plane and finally to $C_{pb}=-0.83$ in a saddle plane of a wavy cylinder.

Before proceeding to examine the drag behavior of wavy cylinders in a cross-flow, the definition of mean drag coefficient used in the present paper has to be clarified. Here, C_D is used to designate the spanwise-averaged mean drag coefficient, so that $(C_D)_{\mathrm{wavy}}$ denotes the average mean C_D for the wavy cylinder and its counterpart for the circular cylinder is $(C_D)_{\mathrm{circular}}$. In the case of a circular cylinder, d_z and d are identical; consequently, either diameter can be used to normalize the mean drag to give $(C_D)_{\mathrm{circular}}$. On the other hand, if a meaningful comparison with $(C_D)_{\mathrm{circular}}$ was to be made, only d should be used to derive $(C_D)_{\mathrm{wavy}}$. Using a load-cell to measure the spanwise-averaged mean drag coefficient of a wavy cylinder, Lam et al. (2004) found that it was generally less than that of a corresponding circular cylinder; a drag reduction of up to 20% was obtained. It would be of interest to determine whether a fairly accurate average $(C_D)_{\mathrm{wavy}}$ could also be obtained by integrating the wake velocity distributions, as suggested by Antonia and Rajagopalan (1990). Different methods can be used to determine $(C_D)_{\mathrm{wavy}}$ using the method of integrating the velocity distributions across the wake. One method is to traverse the wake velocity at a finite number of locations along the whole span; another is to select these locations within one or two wavelengths of the wavy cylinder while a third is to pick four locations within half a wavelength having one location each in the nodal and saddle plane. A subscript i is used to denote the sectional mean drag coefficient C_{Di}. The local behavior is reflected by normalizing C_{Di} by d_z rather than by d. For example, C_{D1} denotes the sectional mean drag coefficient at the nodal plane (see Table 2). The average sectional mean drag in the spanwise direction, after renormalizing by d, over one quarter wavelength (node to saddle) is

Table 1
Summary of formation length at different Reynolds number and cross-section

Cylinder	Formation length	Re = 3000	Re = 6000	Re = 9000
Circular cylinder	L_{fc}	2.25	2.02	1.70
	L_{fu}	2.12	1.90	1.60
Wavy cylinder $z/\lambda=0$ (nodal plane)	L_{fc}	2.96	2.80	2.25
	L_{fu}	2.90	2.61	2.00
Wavy cylinder $z/\lambda=0.167$	L_{fc}	2.98	2.85	2.32
	L_{fu}	2.95	2.70	2.05
Wavy cylinder $z/\lambda=0.333$	L_{fc}	3.07	2.90	2.45
	L_{fu}	3.05	2.80	2.20
Wavy cylinder $z/\lambda=0.500$ (saddle plane)	L_{fc}	3.12	2.95	2.50
	L_{fu}	3.10	2.85	2.30

Table 2
Values of C_D were obtained by integrating the profiles of the mean velocity and the normal Reynolds stresses at x/d=8

Re	Nodal plane $z/\lambda=0$ $d_z/d=1.182$	$z/\lambda=0.167$ $d_z/d=1.091$	$z/\lambda=0.333$ $d_z/d=0.909$	Saddle plane $z/\lambda=0.500$ $d_z/d=0.818$	$(C_D)_{wavy}$	$(C_D)_{circular}$	Drag reduction in %
	C_{D1} $[(C_{D1})d_z/d]$	C_{D2} $[(C_{D2})d_z/d]$	C_{D3} $[(C_{D3})d_z/d]$	C_{D4} $[(C_{D4})d_z/d]$			
3000	0.72 [0.850]	0.76 [0.830]	0.91 [0.827]	0.98 [0.802]	0.82	0.93	11.8
6000	0.75 [0.886]	0.79 [0.862]	0.97 [0.882]	1.09 [0.892]	0.88	0.96	8.3
9000	0.86 [1.016]	0.88 [0.960]	1.02 [0.927]	1.11 [0.908]	0.96	1.08	11.1

taken to be $(C_D)_{wavy}$ in the present analysis. It will be interesting to see if this way of determining $(C_D)_{wavy}$ would also yield a drag reduction as reported by Lam et al. (2004).

The mean drag C_D is given rise by the pressure exerted on the upstream and downstream side of the cylinder. In the subcritical regime, $(C_D)_{circular}$ only changes negligibly; hence C_D is proportional to C_{pb}. Therefore, an elongation of the eddy formation region or a longer formation length in the subcritical regime will give rise to a higher pressure in the rear side of the cylinder, thus leading to a decrease in $(C_D)_{circular}$. Furthermore, a lengthening of the vortex formation region transports eddies away from the base of the cylinder. Since alternate shedding of eddies induces pressure fluctuations on opposite sides of the cylinder, this behavior gives rise to a fluctuating lift. As the eddies move farther away from the base of the cylinder a smaller fluctuating lift is obtained. The result shows that vortex shedding from the wavy cylinder is less vigorous than that from a circular cylinder. This behavior would lead to an increase in base pressure and a decrease in pressure fluctuation, and is why the wavy cylinder exhibits a drag reduction and a suppression of FIV. From Fig. 2, it can be noticed that the maximum reverse flow velocity decreases from the saddle plane to the nodal plane. The maximum reverse flow velocity for a circular cylinder is larger than that of a wavy cylinder in the nodal plane and less than that in the saddle plane. Furthermore, a more rapid velocity recovery from the location where the reverse flow has a maximum value is found in the saddle plane than in other planes. This phenomenon will be analyzed in the next subsection.

Fig. 3 shows the spanwise vortical structures obtained using LIF at Re = 600. The laser sheet and view plane is shown in Fig. 1 and the flow is from left to right. From the figure, it can be observed that the formation length in the wake of the saddle plane is longer than that in the nodal plane, as indicated by the arrows. This 3-D phenomenon can be seen clearly after the Strouhal vortex has just been shed, for example, at $t/T=0.25$ or 1.25. In addition, a rib-like structure was found in the cylinder wake joining neighboring vortices. This is most obvious at $t/T=1.25$. The 3-D rib-like structure could distort the Strouhal vortex filaments. The continuous distortion of vortex filaments led ultimately to their breakdown in the near wake. Gerrard (1978) observed the same distortions of vortex filaments in the wake of a circular cylinder and called them 'fingers' because they were pointed towards the cylinder. In his research, the fingers appeared at randomly disposed spanwise positions and followed each other in succession at the same spanwise position. As Re increased, these fingers appeared in clumps with a larger number of filaments and more frequently at each position. According to the description of 'fingers', it could be postulated that the rib-like structure in the present experiments might have the same structure as 'fingers'. However, the rib-like structure in the wake of a wavy cylinder seems to appear near the saddle planes. Furthermore, the number of structures is constant and is equal to the number of saddles of the cylinder. From the above observation, it could be deduced that the wavy shape caused the present structure of the wake to be different from that behind a circular cylinder. It is quite possible that, unlike a 2-D vortex sheet, the 3-D vortex sheet behind a wavy cylinder is more difficult to roll up into a mature vortex. Therefore, it rolls up at a position further downstream (thus a longer formation length) with a weaker strength. Such vortices then interact and break down through a rib-like structure. As a result, the base pressure is increased and the fluctuation pressure is reduced. This, therefore, results in a reduction of the average mean drag coefficient, $(C_D)_{wavy}$, and the fluctuating lift.

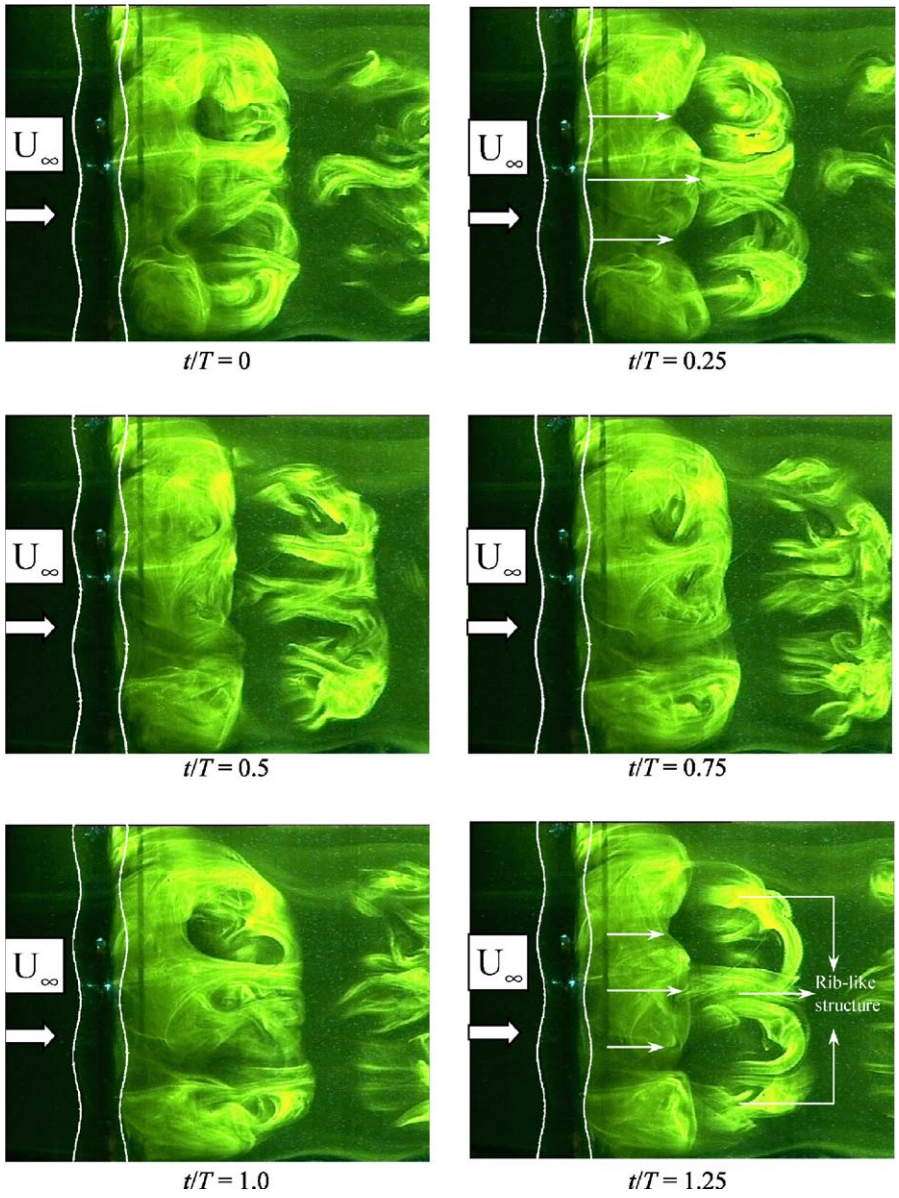

Fig. 3. A time sequences of LIF results on spanwise vortical structure of the wavy cylinder, Re = 600.

3.2. Spanwise variation and three-dimensionality in the wake

Variation of the velocity distributions along the span of the cylinder could highlight the 3-D behavior of the vortex structure behind the wavy cylinder. The purpose of this section is to evaluate the difference in velocity distributions behind a wavy cylinder. Spanwise distributions of U/U_∞ in the $y = 0$ plane are given in Fig. 4. The measuring distance covers two wavelengths and has 100 points evenly distributed within the distance. Three sets of data were obtained at Re = 3000 and they were obtained at $x/d = 1$, 1.5 and 2. These locations are within the wake formation region (Fig. 2). Witnin this region, the negative value of U gradually increases from $x/d = 1$ to $x/d = 2$. From Fig. 4, it is also observed that the negative value of U behind the saddle points is greater than that behind the nodal points. This is clearly evident at $x/d = 2$, which is consistent with the U/U_∞ distribution shown in Fig. 2 along the wake centerline.

The effect of this reverse flow on the development of the streamwise vortices could be gleaned from an examination of the vorticity and streamline field. Figs. 5 and 6 show a time sequence of the instantaneous vorticity contours and

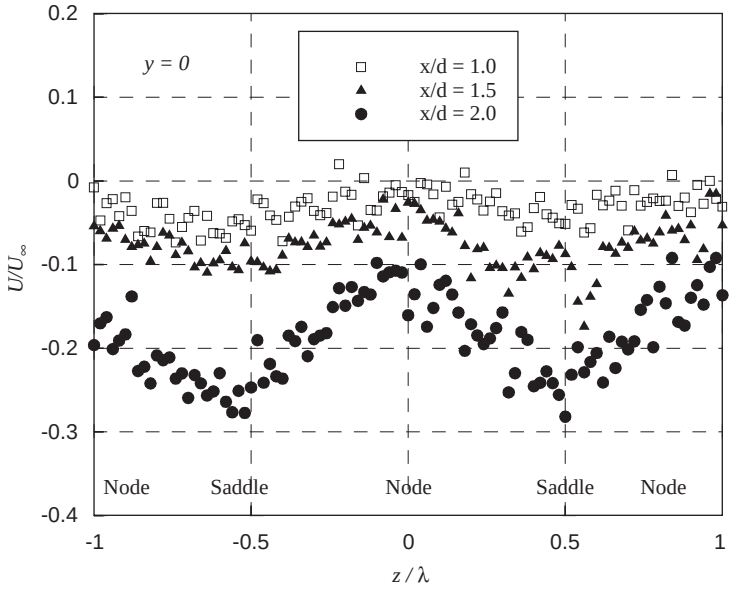

Fig. 4. Spanwise distributions of U/U_∞ at several x/d locations along the line $y=0$, Re = 3000.

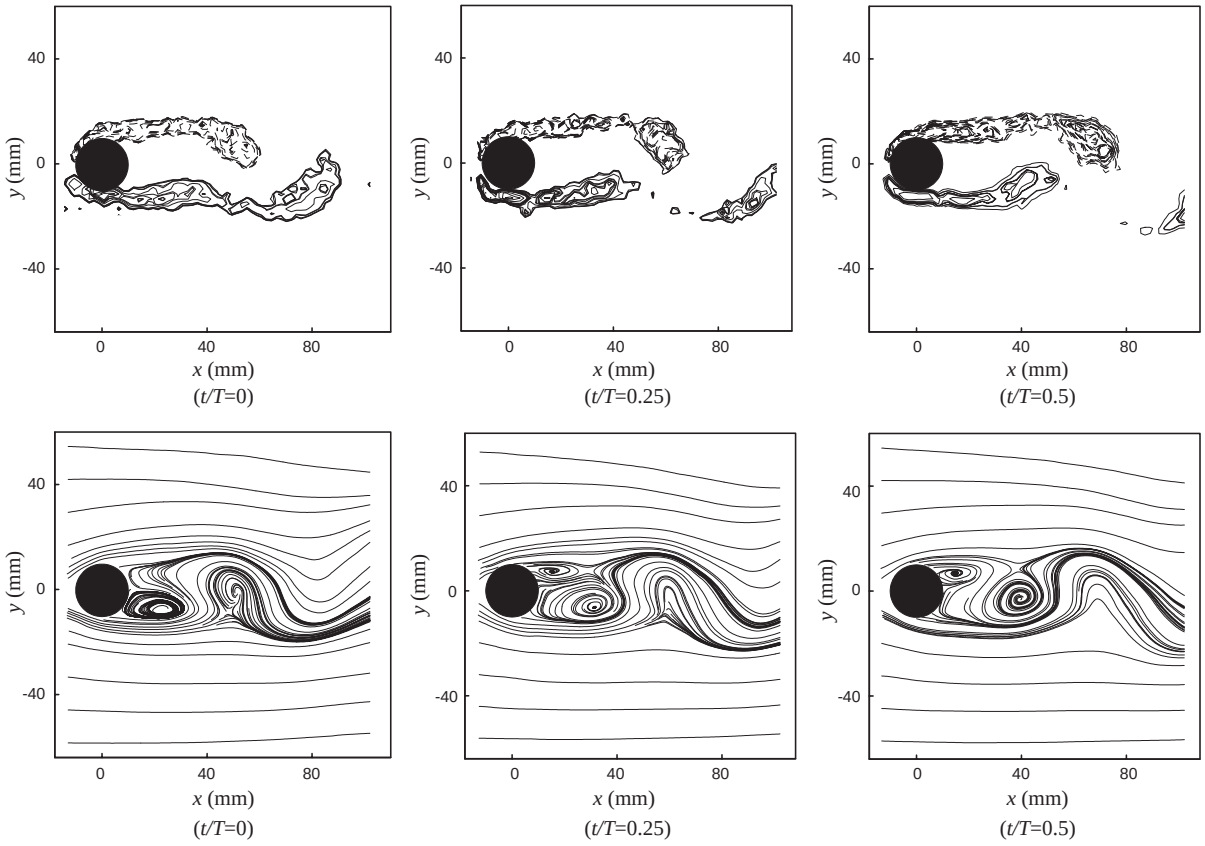

Fig. 5. Consecutive stages of vorticity contours (upper) and streamlines (lower) in the near wake of a nodal plane at Re = 200.

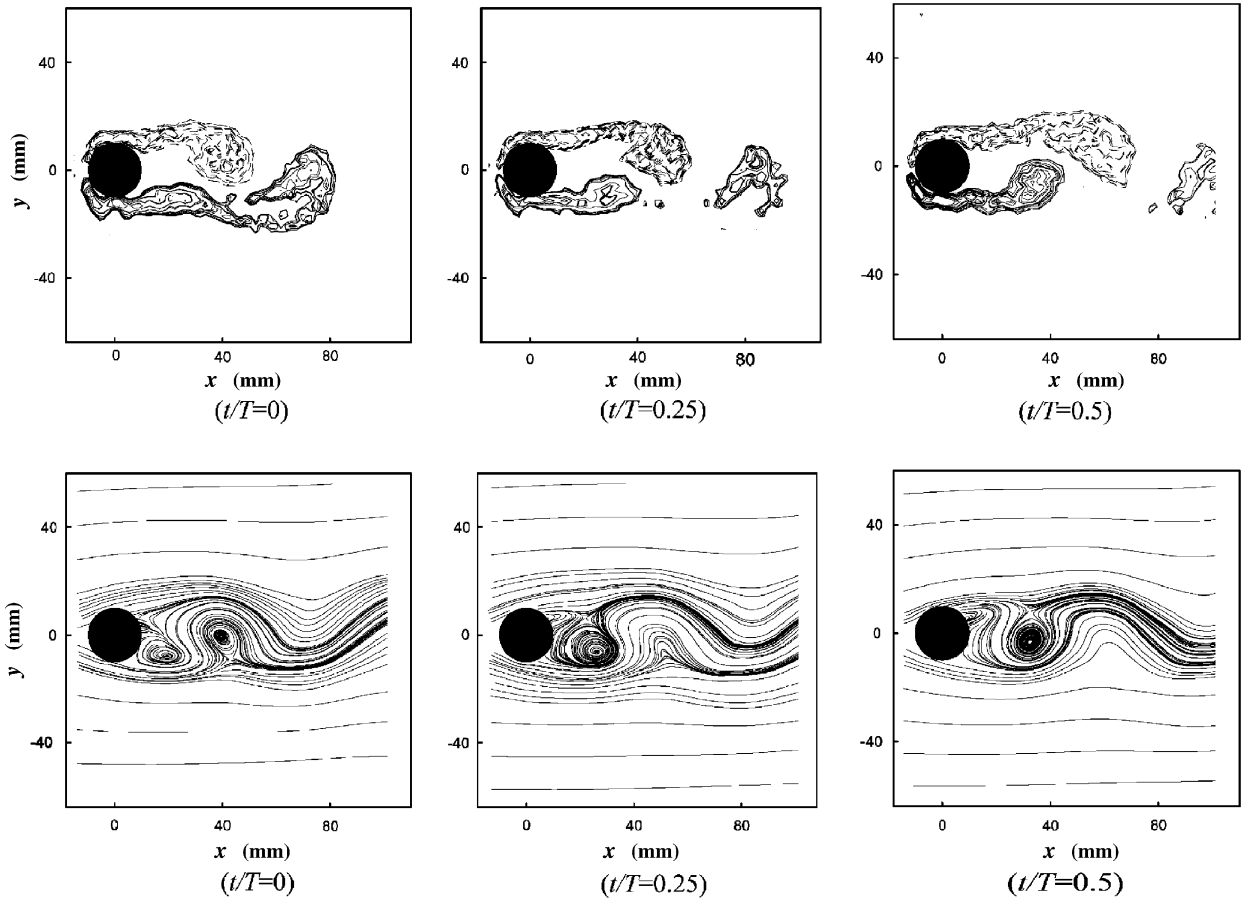

Fig. 6. Consecutive stages of vorticity contours (upper) and streamlines (lower) in the near wake of a saddle plane at Re = 200.

streamlines behind a node and a saddle point, respectively, of the wavy cylinder at Re = 200. These contours and streamlines were obtained by properly processing the PIV particle images. Inspite of the much lower Re, the vorticity structure and streamline map could contribute to an understanding of the general characteristics of the 3-D nature of the vortices behind the wavy cylinder. However, it should be noted that the difference in Re might result in other minor differences in flow characteristics. The vorticity field corresponding to a particular velocity field at a given t/T (where T is the period of vortex shedding) was shown in the upper panel of Figs. 5 and 6, while the corresponding streamline plot was obtained by integrating the velocity field and is shown in the lower panel of Figs. 5 and 6. Bilinear interpolation of the measured velocity was used in the integration. The time interval between consecutive figures is $0.25T$. From the vorticity map, the formation and evolution of two rows of vortices with alternating positive and negative signs can be easily tracked through the three phases shown. The streamline patterns show that the separating free shear layers emanating from the top and bottom side of the wavy cylinder were nearly parallel. It is further found that the vorticity maps show a hook-like structure behind the nodal and the saddle plane. Thus, it could be surmised that reverse flow in the formation region is responsible for this type of hook-like structure.

The high reverse flow (with maximum U/U_∞ reaching -0.3) indicates that the region surrounding $x/d = 2$ is particularly susceptible to the establishment of 3-D behavior as a result of the stretching of the streamwise vorticity in the separated shear layers. To further illustrate this point, the nondimensional spanwise flow component near the edge of the immediate wake, W/U_∞, is presented in Fig. 7. It should be noted that the spanwise velocity component is zero at both the nodal and saddle plane. The results further show that there is a significant spanwise flow from the saddle plane to the nodal plane. This up-slope velocity lends credibility to the interpretation that there is a high degree of three-dimensionality in the wake flow. Fig. 8 illustrates schematically the surface streamlines of a 3-D separation near the separation line. The different separated angles along the span were derived from previous measurements of the pressure distribution on a wavy cylinder with the same parameters [Lam et al. (2004)]. In that experiment, it was shown that separation at the saddle plane occurs much earlier than that at the nodal plane. The maximum negative pressure coefficient shifts from θ=60° at the saddle plane to about 70° at the nodal plane. From Fig. 8, it can be seen that at separation, except at the nodes and saddles, the stream-surface approaches the separation line tangentially and also leaves it tangentially into the flow. Consequently, the free shear layers shed from the points near the saddles are considerably extended along the spanwise direction. On the other hand, the shear layers near the nodes are contracted and the flow of the separated shear layers is accelerated around the nodes. Consequently, 2-D vortex rolling is distorted and the vortices become 3-D in the wake. It could be argued that the longitudinal vorticity component is produced by 3-D separation near the separation line. Thereafter, the 3-D vortex sheet rolls up into a large-scale 3-D vortex, which diffuses and decays along the wake.

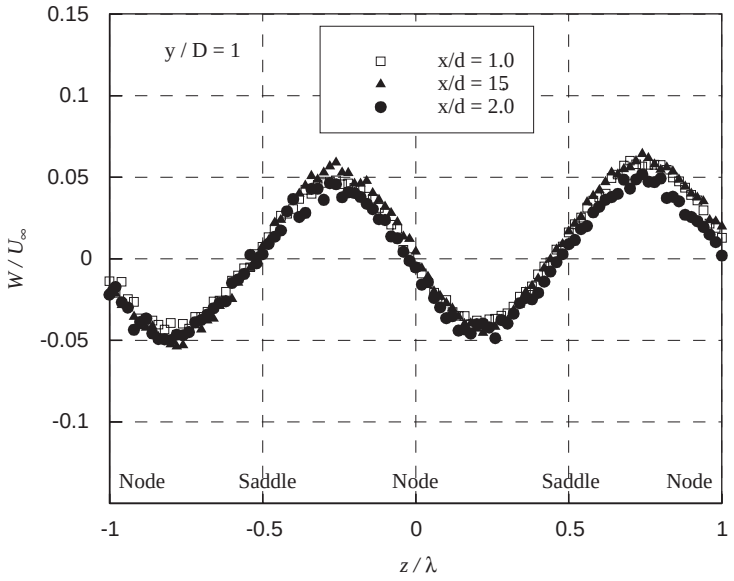

Fig. 7. Spanwise distributions of W/U_∞ at several x/d locations along the line $y/d = 1$, Re = 3000.

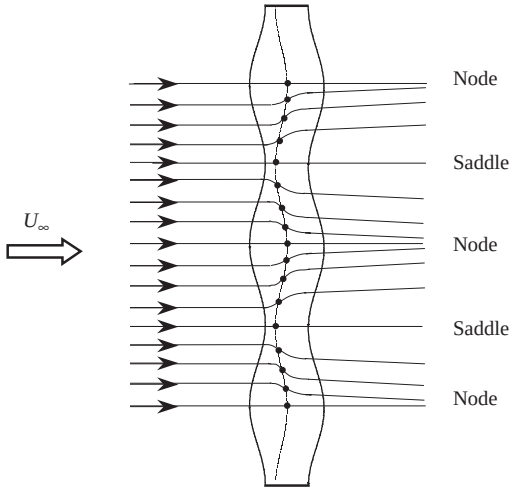

Fig. 8. The surface streamlines of 3-D separation.

3.3. Cross-stream variation in the wake structure

The cross-stream profiles of U/U_∞ in the near wake of the wavy cylinder at Re = 3000, 6000 and 9000 are shown in Fig. 9. The nondimensional distance from the axle center of the wavy cylinder is x/d=3, 5 and 8. Measurements were made at two different span sections, node and saddle, for the purpose of comparison. At Re = 3000 and x/d=3 (Fig. 9(a)), it can be seen that the wake in the saddle plane is wider than that in the nodal plane. Furthermore, the velocity value at $y = 0$ is negative at the saddle plane and positive at the nodal plane. This implies that the flow is still in the reverse flow region at the saddle plane and that the formation length is longer in this plane than that in the nodal plane. As Re increases, the width of the near wake does not show any increase compared to that at x/d=3 (compared Fig. 9(a) with Figs. 9(b) and (c)). This is a consequence of a decrease in the formation length as Re increases, hence x/d=3 is outside the formation region at Re = 6000 and 9000. Beyond the formation length, at x/d=5, the wake at the nodal plane is wider than that at the saddle plane; a consequence of 3-D vortex interaction and the entrainment of the main flow. The wake width becomes essentially the same as x/d increases. Furthermore, the difference between the velocities at $y = 0$ at the nodal and saddle plane decreases as Re increases. This seems to indicate that velocity recovery in the saddle plane is faster than that in the nodal plane. Considering the higher reverse flow velocity in the saddle plane, it is reasonable to argue that vortex shedding in the saddle plane brings greater entrainment than in the nodal plane. This, in turn, is responsible for the relatively faster recovery of U.

Typical flow patterns in the near wake of a nodal plane are shown in Fig. 10. The Re for these patterns is 200, 400, 600, 800, 1500 and 2000, respectively. Unlike the flow pattern of a circular cylinder, the vortex shape behind the wavy cylinder curved up like a balloon. This feature was also found in the near wake of a saddle plane, shown in Fig. 11. From Figs. 10 and 11, it was evident that the near wake in the saddle plane is wider than that in the nodal plane. Although, the LIF experiments were carried out at relatively low Re, the results were consistent with those deduced from velocity distribution measurements at higher Re shown in the sections above; namely, the wake width is wider at the saddle plane than at the nodal plane before the formation length. Normally, a wider wake accompanies an earlier vortex separation. Therefore, separation at the saddle plane is earlier than at the nodal plane could also be identified from flow visualization pictures. According to the above observation, two characteristics are noticeable in the flow structure: (i) free shear layer separation at the saddle plane is earlier than that at the nodal plane ($\alpha_s < \alpha_n$, where α_s denotes the separation angle at the saddle plane and α_n denotes the separation angle at the nodal plane); and (ii) the wake at the saddle plane is wider and longer than that at the nodal plane. A sketch of this 3-D flow structure is postulated in Fig. 12.

3.4. Reynolds stresses in the wake

Distributions of the Reynolds stresses measured at three different x/d locations are shown in Fig. 13. Since the measurements in the range of Re = 3000–9000 are basically similar, only the results of Re = 6000 are shown in Fig. 13. The profiles of $\overline{u^2}$, $\overline{v^2}$, and $\overline{uv}$ are given in Figs. 13(a), (b) and (c), respectively. All Reynolds stresses are normalized by

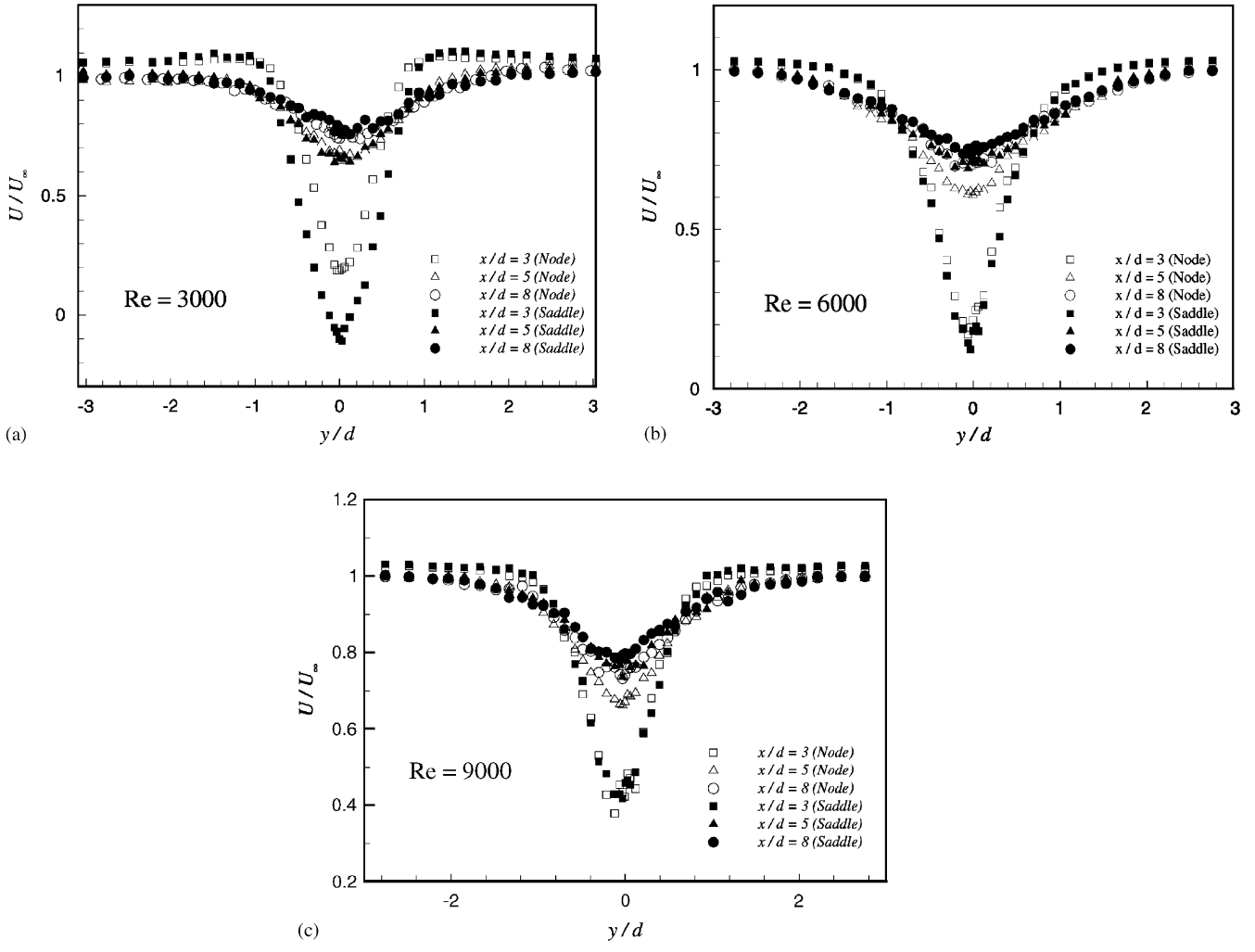

Fig. 9. Comparison of the mean velocity distributions between a nodal and a saddle plane in the wake of the wavy cylinder. (a) Re = 3000, (b) Re = 6000, (c) Re = 9000.

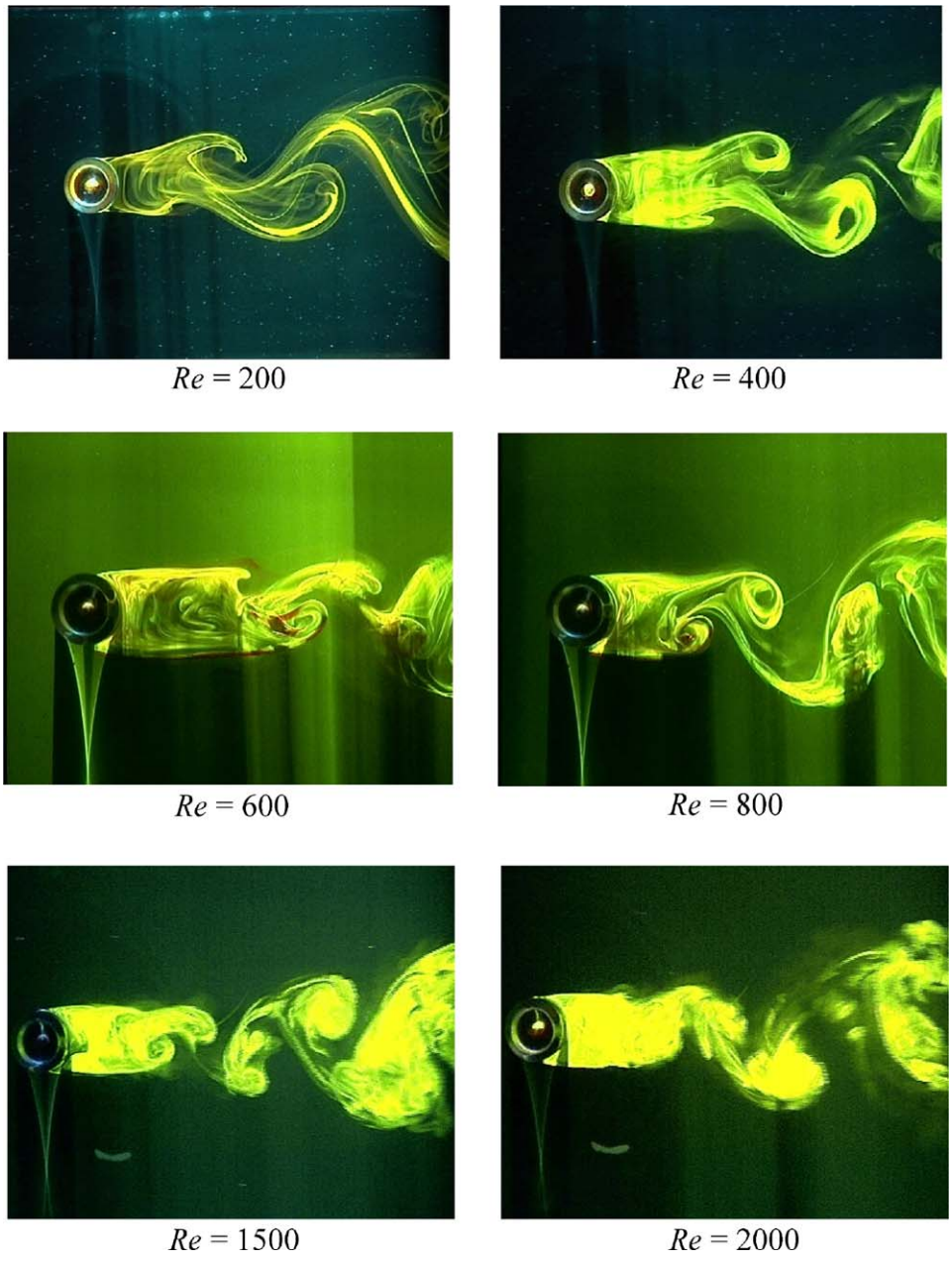

Fig. 10. Flow pattern in the near wake of a nodal plane at Re = 200–2000.

$(U_\infty - U_c)^2$, where U_c is the streamwise velocity at the centerline ($y = 0$), which varies with x. The measured Reynolds stresses in the wake behind a circular cylinder were also included in the figure for comparison. From the figure, it can be seen that the measured normal stresses ($\overline{u^2}, \overline{v^2}$) of the circular cylinder are much higher than that of the wavy cylinder at all x locations examined. Zhou and Antonia (1994) studied a turbulent near-wake in terms of critical points. They referred to the region around the vortex centers as focal region and the region around saddle points between two consecutive vortices as the saddle region. Actually, the focal region represents the large-scale vortical motion of the vortex. They found that saddle point regions associated with spanwise vortices provide a dominant contribution to the Reynolds shear stress, $\overline{uv}$, and the focal region contributed most to $\overline{u^2}$ and $\overline{v^2}$. The significant increase in $\overline{u^2}$ and $\overline{v^2}$,

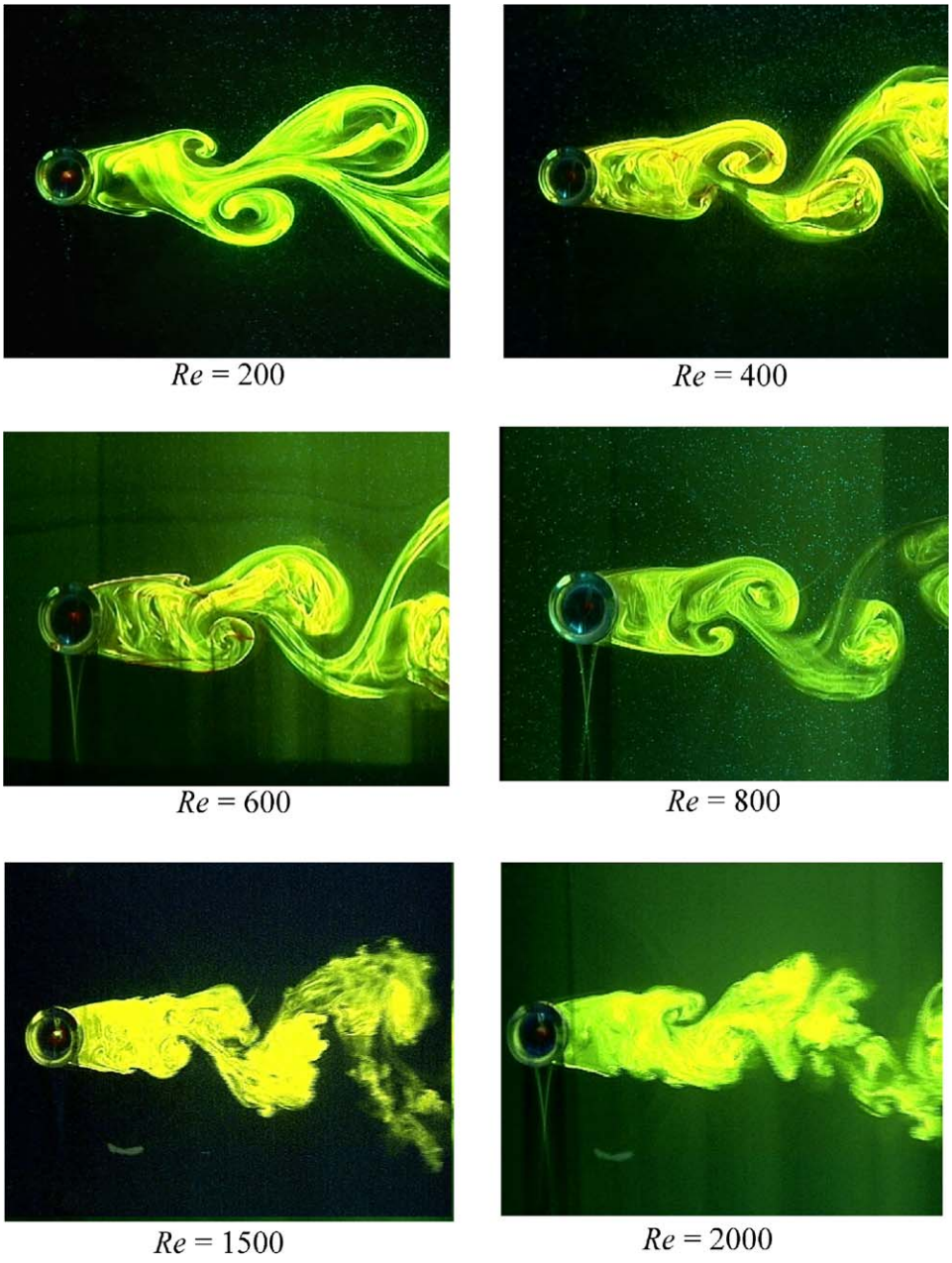

Fig. 11. Flow pattern in the near wake of a saddle plane at Re = 200–2000.

therefore, implies that the two alternating vortex motion are different in the wake of the circular cylinder and the wavy cylinder. In other words, the vortex streets in the circular cylinder wake are more regular.

It is a well known fact that convection of the organized alternating vortices through corresponding sections of the wake will give rise to an "M" shape in the longitudinal Reynolds stress, $\overline{u^2}$. The distance between the two peaks corresponds to the distance between the kernels of the two rows of alternating vortices. Therefore, as the wake becomes more developed, this double peak behavior in $\overline{u^2}$ will become less and less prominent until its disappearance at a certain downstream section. For example, So et al. (2000) measured the turbulence field of a circular cylinder and found that the disappearance of the double peak occurs after $x/d = 10$; by $x/d = 20$, the peaks have essentially vanished. From the

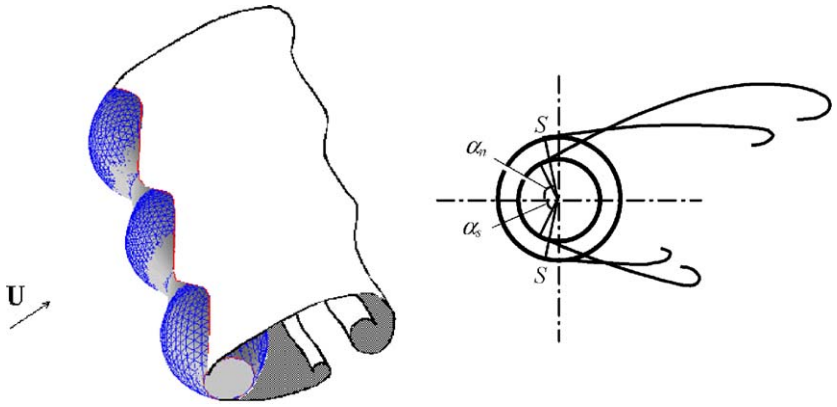

Fig. 12. A conceptual diagram showing the 3-D wake structures being visualized. α_s denotes the separating angle at saddle plane; α_n denotes the separating angle at nodal plane; S denotes the separation points.

present results (Fig. 13(a)), it was found that disappearance of the double peak in the wake of the wavy cylinder occurs much earlier. In fact, the peaks essentially vanished after $x/d=5$ at the nodal plane and after $x/d=8$ at the saddle plane. These results substantiate the earlier inference that the wake behind a wavy cylinder is 3-D and indicate that three-dimensionality leads to much earlier breakdown of large-scale coherent vortex structure. This phenomenon further implies that the alternately shed vortices in the wake of a wavy cylinder have less fluctuating kinetic energy induced by the enhanced mixing due to turbulence. For the same reason, it is noted that turbulence mixing decreases from the nodal plane to the saddle plane at the same x/d.

Fig. 13(b) shows the distributions of the transverse Reynolds stress, $\overline{v^2}$. It can be seen that the maximum amplitude of the $\overline{v^2}$ component always appears at the $y=0$ plane regardless of the cylinder shape. This indicates that $\overline{v^2}$ is equally affected by the alternating vortex streets shed at the nodal and saddle plane. The maximum difference in $\overline{v^2}$ between the circular cylinder and the wavy cylinder occurs at $x/d=3$. However, this difference decreases as x/d increases. Considering the fact that U_c of the wavy cylinder is close to zero at $x/d=3$, it is reasonable to argue that the large $(U_\infty - U_c)^2$ is responsible for the large difference of $\overline{v^2}$ between the wavy and circular cylinder at $x/d=3$. As shown in Table 1, L_{fc} at $\mathrm{Re}=6000$ in the nodal plane is about 2.80, while in the saddle plane it is about 2.95. It could be concluded that, at $x/d=3$, the vortices have larger effects in the nodal plane. This is why $\overline{v^2}$ in the saddle plane at $x/d=3$ is smaller than that in the nodal plane. After the vortex formation process has completed, for example at $x/d=5$, the high fluctuating kinetic energy of the alternating vortex streets and the low turbulence mixing contributed to a larger $\overline{v^2}$ in the saddle plane. The difference between $\overline{v^2}$ measured at the different planes decreases further downstream as the wake becomes more developed.

The shear stress profiles are shown in Fig. 13(c). In general, they show an anti-symmetric character; the two extrema are the result of the passage of the cores of the organized alternating vortices. From the figure, it can be seen that the $\overline{uv}$ distributions for the wavy and circular cylinder are essentially identical except at $x/d=3$, where U_c of the wavy cylinder is close to zero.

According to Antonia and Rajagopalan (1990) and Dam (1999), the mean drag coefficient C_D can be determined from the distributions of the mean velocity and Reynolds normal stresses across the wake. In the present investigation, the profiles of the mean streamwise velocity and the Reynolds normal stresses at x/d=8 are used to calculate $(C_D)_{\mathrm{wavy}}$. The values of the C_{Di} at different spanwise sections of the wavy cylinder are also given in Table 2. These are calculated for the three Re examined and listed in Table 2 for comparison with the corresponding $(C_D)_{\mathrm{circular}}$. In order to compare the various C_D on the same basis, the sectional C_D is renormalized by d and the results are listed in Table 2 as bracketed values under C_{Di}. Thus, $(C_D)_{\mathrm{wavy}}$ is approximated by the average of the four bracketed values under C_{Di}. From the table, it is can be seen that C_{Di} at the saddle plane is greater than that at the nodal plane due largely to the spanwise variation in d_z. Once C_{Di} is corrected by normalizing it with d, a trend of decreasing C_{Di} from the nodal plane to the saddle plane is noted. This result shows that, as far as the mean drag is concerned, a periodic variation along the span can be assumed. Finally, it should also be noted that $(C_D)_{\mathrm{wavy}}$ is less than $(C_D)_{\mathrm{circular}}$ for all Re tested. Therefore, it can be concluded that $(C_D)_{\mathrm{wavy}}$ obtained by integrating the velocity distributions across the wake at four locations within one half wavelength yields a reasonable average mean drag for the wavy cylinder. The $(C_D)_{\mathrm{wavy}}$ thus determined also shows a drag reduction in the Re range of 3000–9000. Therefore, this set of data supplements the force measurements of Lam et al. (2004) in the Re range of 10 000–60 000.

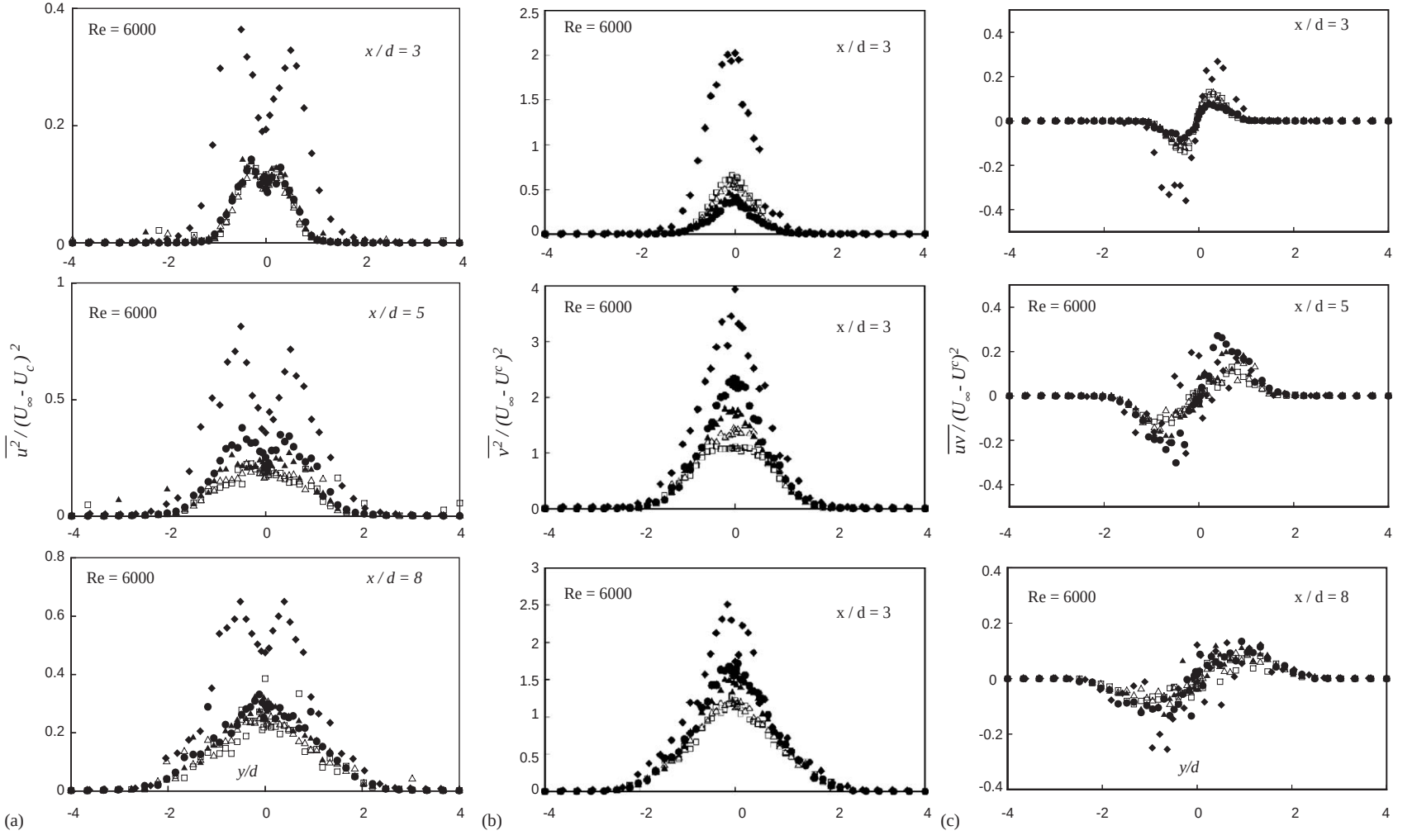

Fig. 13. Comparison of the Reynolds stress distributions at Re = 6000, Figure (a), (b) and (c) give the profiles of $\overline{u^2}$, $\overline{v^2}$, $\overline{uv}$, respectively: □, nodal plane of wavy cylinder ($z/\lambda = 0$), △, wavy cylinder, $z/\lambda = 0.167$, ▲, wavy cylinder, $z/\lambda = 0.333$, ●, saddle plane of wavy cylinder ($z/\lambda = 0.500$), ♦, circular cylinder.

4. Conclusions

In this paper, the wake velocity field including the distributions of the mean velocity, the normal stresses and the shear stress along the x-, y- and z-direction as well as the flow patterns of a wavy cylinder obtained through the use of LDA, LIF and DPIV measurements were investigated in detail.

In the first part, the longitudinal evolution of mean velocity and r.m.s. values of the fluctuating streamwise velocity along the wake centerline of the wavy cylinder at four cylinder span sections from a node to a saddle were measured. Similar measurements on a circular cylinder were also obtained. The results indicate that the average vortex formation length to over half a wave length of the wavy cylinder is longer than that of the circular cylinder in the Re range from 3000 to 9000. It appears that there is a direct link between the long formation length and the resulting drag reduction and vibration suppression. The lengthening of the vortex formation region leads to a corresponding decrease in $(C_D)_{\text{wavy}}$ and the associated fluctuating lift. Furthermore, the LDA and LIF measurements show that the formation length in the saddle plane is longer than that in the nodal plane. Once C_{Di} in these planes is corrected to base on d rather than d_z, the C_{Di} behavior is consistent with the measured formation length in the saddle and nodal plane and with the observation pertaining to $(C_D)_{\text{wavy}}$.

Results of the velocity distributions along the spanwise location of the wavy cylinder show the reverse flow speed in the vortex formation region of the saddle plane is higher than in the nodal plane, which is responsible for the hook-like structure of the vorticity in the saddle plane, shown in the vorticity contour map obtained by DPIV. The spanwise velocity results in the outside region of the separated shear layers show that the flow is from the saddle plane to the nodal plane. Consequently, the shear layers shed from the points near the saddles extend along the spanwise direction, while the shear layers near the nodes contract and the flow of the separated shear layers accelerates around the nodes. As a result, 2-D vortex rolling is distorted and a 3-D vortex structure is formed.

The cross-stream profiles of U and the LIF results show that the wake in the formation region of the saddle plane is wider than that of the nodal plane. It was further found that separation at the saddle plane is earlier than at the nodal plane. An interpretation of this 3-D flow structure is postulated and a sketch was drawn.

Analysis of the Reynolds stresses shows the vortex streets in the circular cylinder wake are more regular, while the wavy cylinder wake shows more irregularity. Three-dimensional vortex structure will breakdown much more readily when they interact with each other. This is further verified by the earlier disappearance of the double peaks in the $\overline{u^2}$ distribution. The measured Reynolds stresses also show that turbulence mixing within the vortex street in the nodal plane is larger than that in the saddle plane. The velocity and Reynolds stress distributions further provide an important database for the validation of turbulence modelling and 3-D numerical simulations.

Acknowledgements

This work was fully supported by a grant from the Research Grants Council of the Hong Kong Special Administrative Region, China (Project No. PolyU 5154/00E).

References

Ahmed, A., Bays-Muchmore, B., 1992. Transverse flow over a wavy cylinder. Physics of Fluids A4, 1959–1967.

Ahmed, A., Khan, M.J., Bays-Muchmore, B., 1993. Experimental investigation of a three-dimensional bluff-body wake. AIAA Journal 31, 559–563.

Antonia, R.A., Rajagopalan, S., 1990. Determination of drag of a circular cylinder. AIAA Journal 28, 1833–1834.

Bearman, P.W., 1965. Investigation of the flow behind a two-dimensional model with a blunt trailing edge and fitted with splitter plates. Journal of Fluid Mechanics 21, 241–255.

Bearman, P.W., Owen, J.C., 1998. Suppressing vortex shedding from bluff bodies by the introduction of wavy separation lines. In: Proceedings of the 1998 ASME Fluids Engineering Division Summer Meeting, Washington, DC, FED-Vol. 245, Session 191-09, FEDSM98-5190.

Bloor, S., 1966. The transition to turbulence in the wake of a circular cylinder. Journal of Fluid Mechanics 19, 290–304.

Braza, M., Faghani, D., Persillon, H., 2001. Successive stages and the role of natural vortex dislocations in three-dimensional wake transition. Journal of Fluid Mechanics 439, 1–41.

Cooke, J.C., Robins, A.J., 1970. Boundary-layer flow between nodal and saddle points of attachment. Journal of Fluid Mechanics 41, 823–835.

Crickmore, R.I., Jack, S.H., Hann, D.B., Greated, C.A., 1999. Laser doppler anemometry and the acousto-optic effect. Optics & Laser Technology 31, 85–94.

Dam, C.P. Van, 1999. Recent experience with different methods of drag prediction. Progress in Aerospace Sciences 35, 751–798.
Davey, A., 1961. Boundary-layer flow at a saddle point of attachment. Journal of Fluid Mechanics 10, 593–610.
Duck, P.W., 1979. Flow induced by a torsionally oscillating wavy cylinder. Quarterly Journal of Mechanics and Applied Mathematics 32, 73–91.
Gerrard, J.H., 1978. Wakes of cylindrical bluff bodies at low Reynolds-number. Philosophical Transactions of the Royal Society of London Series A—Mathematical, Physical and Engineering Sciences 288, 351–382.
Govardhan, R., Williamson, C.H.K., 2001. Mean and fluctuating velocity fields in the wake of a freely-vibrating cylinder. Journal of Fluids and Structures 15, 489–501.
Howarth, L., 1951. The boundary layer in three dimensional flow—Part I: derivation of the equations for flow along a general curved surface. Philosophical Magazine Serials 7, 239–243.
Kerczek, C. Von, 1988. The symmetry plane boundary layer on a corrugated cylinder in cross flow. AIAA Paper No. AIAA-88-3544-CP.
Keser, H.İ., Ünal, M.F., Bearman, P.W., 2001. Simulation of wake from a circular cylinder with spanwise sinusoidal waviness. In: Proceedings of the Second International Conference on Vortex Methods, Istanbul, Turkey, pp. 131–137.
Lam, K., Wang, F.H., Li, J.Y., So, R.M.C., 2004. Experimental investigation of the mean and fluctuating forces of wavy (varicose) cylinders in a cross-flow. Journal of Fluids and Structures, 19, 321–334.
Naumann, A., Morsbach, M., Kramer, C., 1966. The conditions of separation and vortex formation past cylinders. In: NATO AGARD Conference Proceedings in Separated Flow, Vol. 4, pp. 539–574.
Noca, F., Park, H.G., Gharib, M., 1998. Vortex formation length of a circular cylinder ($300 < Re < 4{,}000$) using DPIV. In: Proceedings of the 1998 ASME Fluids Engineering Division Summer Meeting, Washington, DC, FED-Vol. 245, FEDSM98-5149.
Norberg, C., 1986. Interaction between freestream turbulence and vortex shedding for a single tube in cross-flow. Journal of Wind Engineering and Industrial Aerodynamics 23, 501–514.
Norberg, C., 1998. LDV-measurements in the near wake of a circular cylinder. In: Proceedings of the 1998 ASME Fluids Engineering Division Summer Meeting, Washington, DC, FED-Vol. 245, FEDSM98-5202.
Owen, J.C., Bearman, P.W., 2001. Passive control of VIV with drag reduction. Journal of Fluids and Structures 15, 597–605.
Petrusma, M.S., Gai, S.L., 1994. The effect of geometry on the base pressure recovery of segmented blunt trailing edges. Aeronautical Journal 98, 267–274.
Rodriguez, O., 1991. Base drag reduction by the control of three-dimensional unsteady vortical structures. Experiments in Fluids 11, 218–226.
So, R.M.C., Zhou, Y., Liu, M.H., 2000. Free vibrations of an elastic cylinder in a cross flow and their effects on the near wake. Experiments in Fluids 29, 130–144.
Sumner, D., Price, S.J., Paidoussis, M.P., 2000. Flow-pattern identification for two staggered circular cylinders in cross-flow. Journal of Fluids and Structures 411, 263–303.
Tanner, M., 1972. A method of reducing the base drag of wings with blunt trailing edges. Aeronautical Quarterly 23, 15–23.
Tombazis, N., Bearman, P.W., 1997. A study of three-dimensional aspects of vortex shedding from a bluff body with a mild geometric disturbance. Journal of Fluid Mechanics 330, 85–112.
Woo, H.G.C., Cermak, J.E., Peterka, J.A., 1983. On vortex locking-on phenomenon for a cable in linear shear-flow. Journal of Wind Engineering and Industrial Aerodynamics 14, 289–300.
Yang, X., Zebib, A., 1989. Absolute and convective nature of instability in two dimensional wakes at low Reynolds number. Physics of Fluids A—Fluid Dynamics 1, 689–696.
Zhang, J.F., Dalton, C., 1998. A three-dimensional simulation of a steady approach flow past a circular cylinders at low Reynolds number. International Journal for Numerical Methods in Fluids 26, 1003–1022.
Zhou, Y., Antonia, R.A., 1994. Critical points in a turbulent near wake. Journal of Fluid Mechanics 275, 59–81.